Supplemental Material

Femto-second Laser Induced Reversal in In-Plane Magnetized Spin Valves

Jun-Xiao Lin,[1] Yann Le Guen,[1] Julius Hohlfeld,[1] Junta Igarashi,[1] Quentin Remy,[2] Jon Gorchon,[1] Grégory Malinowski,[1] Stéphane Mangin,[1,3] Thomas Hauet[1] and Michel Hehn*[1,3]

[1]*Université de Lorraine, CNRS, Institut Jean Lamour, F-54000 Nancy, France*
[2]*Department of Physics, Freie Universität Berlin, 14195 Berlin, Germany*
[3]*Center for Science and Innovation in Spintronics, Tohoku University, Sendai, Japan*

*Authors to whom correspondence should be addressed: michel.hehn@univ-lorraine.fr

S1. All-optical switching of in-plane magnetized $Co_{20}Ni_{80}$ single layer without the $Co/Gd_{33}Co_{67}$ layer

Let us now investigate the all-optical switching (AOS) phenomenon exhibited by the $Co_{20}Ni_{80}$ (3 nm) layer itself under the influence of a single pulse. Fig. S1 illustrates changes in the longitudinal magneto-optic Kerr effect (MOKE) image after laser pulse excitations at two distinct injected laser fluences. The sample was initialized in the P^+ configuration and subjected to six single pulses. The outcomes indicate the emergence of only a multidomain state, irrespective of the pulse fluence. Consequently, we attribute the observed reversal of the ferromagnetic (FM) layer in the spin valve to the dynamic long-range coupling originating from the GdCo layer, specifically the spin currents generated from the Gd sublattice [1-4].

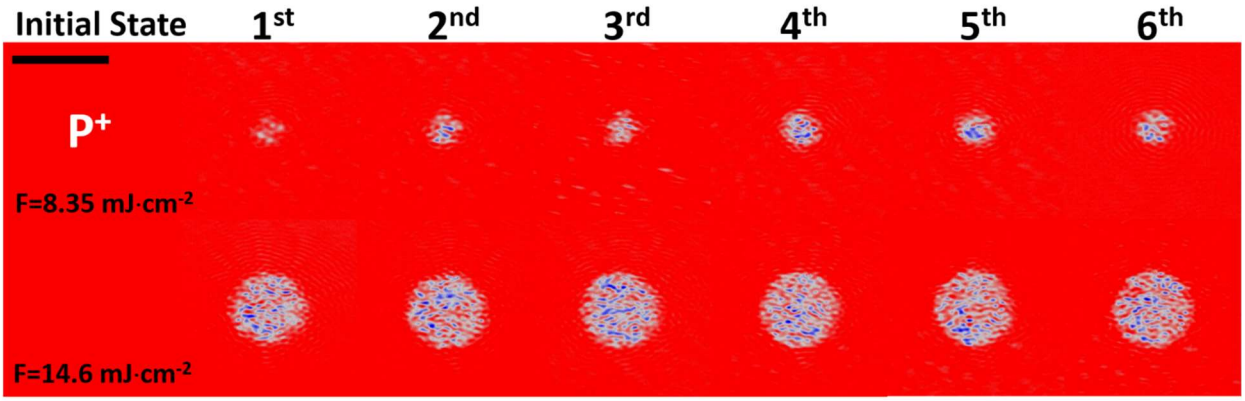

FIG. S1. Kerr images captured after laser excitations with different pulse fluences for the Si substrate/Ta (3 nm)/Cu (5 nm)/$Co_{20}Ni_{80}$ (3 nm)/Cu (5 nm)/Pt (3 nm) sample. A scale bar of 100 μm is provided for reference.

S2. Laser pulse fluence-dependent AOS measurements on Co (3 nm)/$Gd_{33}Co_{67}$ (5 nm)/Cu (10 nm)/$Co_{20}Ni_{80}$ (3 nm) spin valve

We have demonstrated that the Glass/Ta (3 nm)/Co (3 nm)/Gd-rich $Gd_{33}Co_{67}$ (5 nm)/Cu (10 nm)/$Co_{20}Ni_{80}$ (3 nm)/Pt (3 nm) presents optimal AOS behavior. To further understand the influence of pulse fluence on configuration changes associated with switching the $Co_{20}Ni_{80}$ (3 nm) layer, we studied the effect of varying pulse numbers and pump fluence. In Fig. S2, starting from an initial state in the P^+ configuration, six single pulses at a given laser fluence were applied to the sample. The time interval between each pulse was set to 60 seconds. These experiments were repeated for various pump pulse fluences. The results show that partial switching (AP^- state) consistently occurs after the first pulse excitation, regardless of the pulse fluence. A second pulse is always required to achieve full reversal of the $Co_{20}Ni_{80}$ (3 nm) layer.

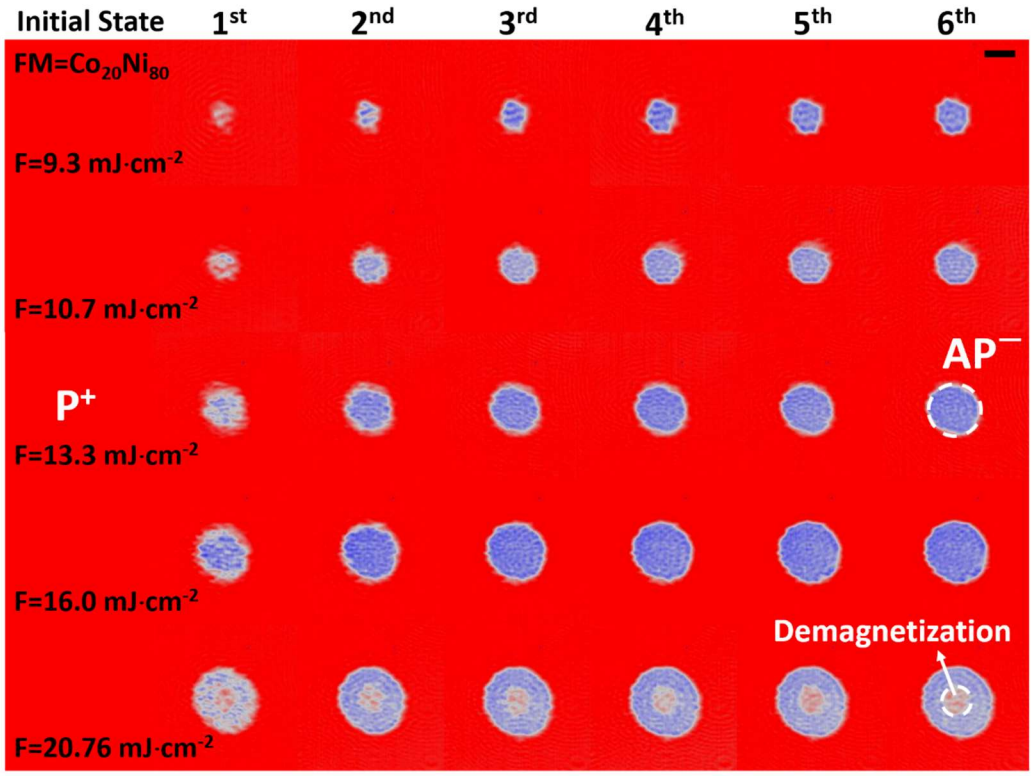

FIG. S2. Longitudinal MOKE images obtained following six individual femtosecond laser pulses with varying pump pulse fluences, inducing AOS in in-plane magnetized Co (3 nm)/Gd-rich $Gd_{33}Co_{67}$ (5 nm)/Cu (10 nm)/$Co_{20}Ni_{80}$ (3 nm) spin valve, starting from the P^+ configuration. A scale bar of 100 μm is included.

S3. Laser pulse fluence-dependent switched domain size for different Co (3 nm)/$Gd_{33}Co_{67}$ (5 nm)/Cu (10 nm)/FM layer (3 nm) spin valves

Fig. S3 illustrates the switched domain size for various FM layers in the Co (3 nm)/Gd-rich $Gd_{33}Co_{67}$ (5 nm)/Cu (10 nm)/an FM layer (3 nm) spin valves as a function of pulse fluence. Increasing the number of pulses only enlarges the reversed domain size, reaching saturation after five pulse excitations. For the FM=$Co_{20}Ni_{80}$, exposing the sample to a fluence as low as 9.3 mJ×cm^{-2} allows to switch only a small region at the center of the pump laser spot, where the laser fluence density is highest. On the other hand, subjecting the sample to a higher pulse fluence, such as 20.76 mJ×cm^{-2}, induces multidomain formation at the center of the circular reversed domain, leading to a reduction in the size of the switched area, as demonstrated in Fig. S2 for F=16 mJ×cm^{-2}. Similar measurements were conducted on spin valves with $Co_{40}Ni_{60}$ and CoFeB as the FM layer, also showing full reversal.

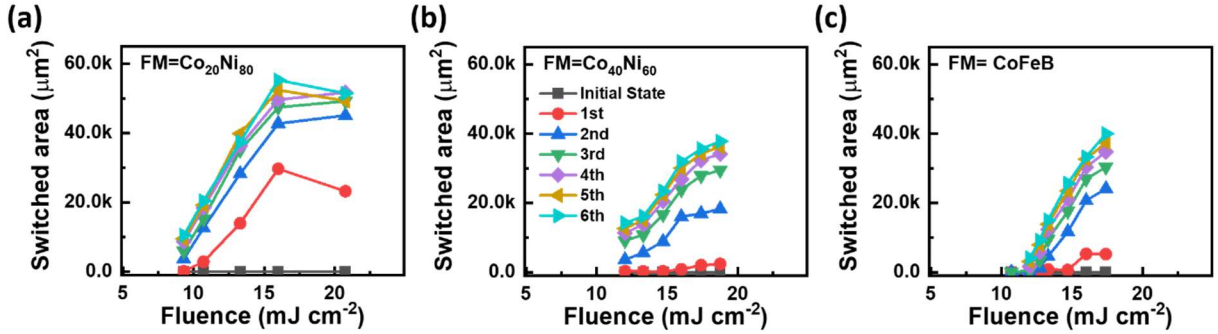

FIG. S3. The averaged switched domain size for varying pulse numbers as a function of pulse fluence. These measurements were performed on spin valves where the FM layer is (a) $Co_{20}Ni_{80}$, (b) $Co_{40}Ni_{60}$, and (c) $Co_{40}Fe_{40}B_{20}$, respectively.

S4. Temperature dependence of saturation magnetization and the corresponding fit for CoFeB layers with different thicknesses

We have measured the temperature dependence of saturation magnetizations, M_S (T), for the Glass/Ta (3 nm)/$Gd_{25}Co_{75}$ (5 nm)/Cu (5 nm)/$Co_{40}Fe_{40}B_{20}$ (t nm)/Pt (3 nm) samples. Fig. S4 depicts the representative M_S (T) curves for samples with various t values. The M_S (T) data is fitted to a $T^{1/3}$ power law equation: $M_S(T)=M_S(0)\times(1-(\frac{T}{T_C}))^{\frac{1}{3}}$, where M_S (0) represents the M_S at T=0 K and T_C denotes the Curie temperature, respectively [5]. The solid lines in Fig. S4 show the best fit curves for the samples. The T_C can be determined by fitting the measured M_S (T) results, corresponding to the temperature at which M_S=0 kAm^{-1}.

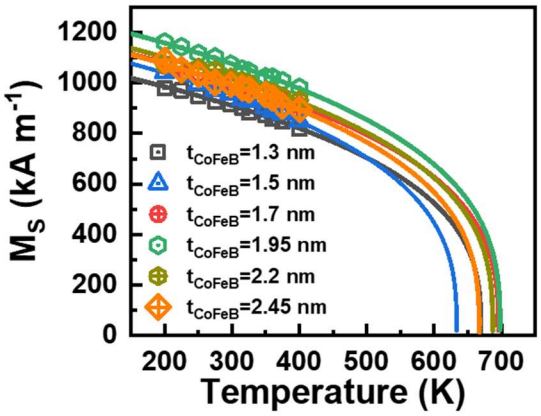

FIG. S4. The temperature dependence of saturation magnetization for different CoFeB thicknesses. The solid lines represent the fit of $T^{1/3}$ power law: $M_S(T)=M_S(0)\times(1-(\frac{T}{T_C}))^{\frac{1}{3}}$, to the measured data.

S5. Longitudinal MOKE hysteresis loops of in-plane magnetized $Gd_{25}Co_{75}$ (5 nm)/Cu (5 nm)/CoFeB (t nm) spin valves

For longitudinal MOKE hysteresis loop measurements, microscopy was conducted through the CoFeB thin film side. In this configuration, the MOKE signal of CoFeB exceeded that of the Gd-rich $Gd_{25}Co_{75}$ layer. This configuration effectively enhances the Kerr signals of these ultrathin CoFeB layers and aids in the interpretation of AOS measurements. The obtained MOKE hysteresis loops for samples with different t values are presented in Fig. S5. The results reveal a square-shaped profile in all MOKE loops and the presence of four distinguishable magnetic states among the samples. Moreover, the findings indicate that the coercivity of CoFeB consistently remained smaller than that of the $Gd_{25}Co_{75}$ layer and emphasize the absence of exchange coupling between the two magnetic layers.

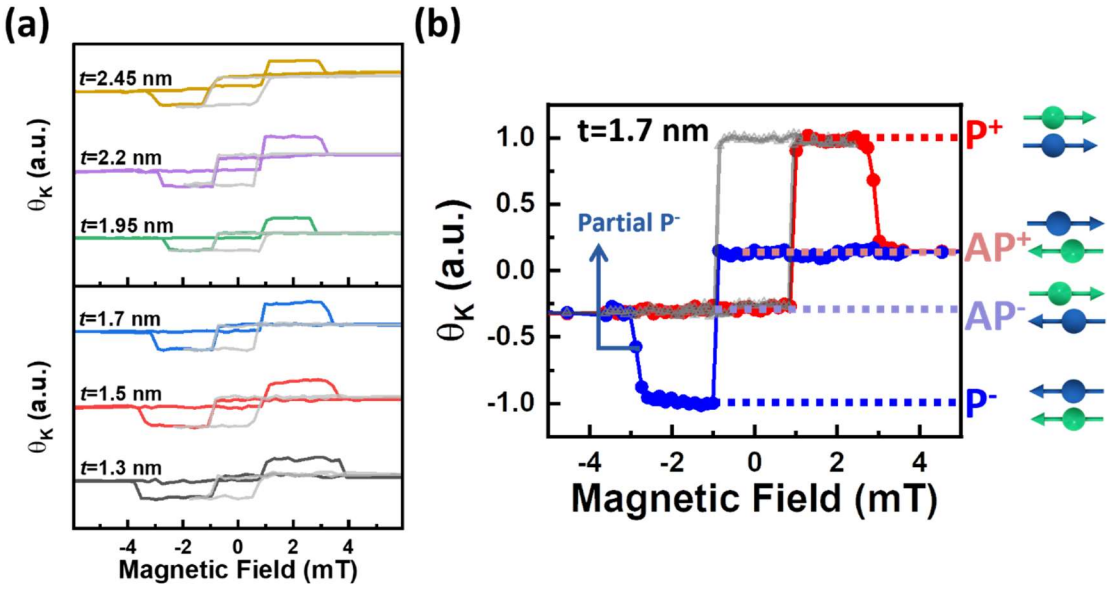

FIG. S5. (a) Longitudinal MOKE hysteresis loops with minor loops (corresponding to the CoFeB) for the Gd-rich $Gd_{25}Co_{75}$ (5 nm)/Cu (5 nm)/CoFeB (t nm) spin valves. (b) Normalized hysteresis loops for the spin valve with t of 1.7 nm and the corresponding four magnetic configurations. The blue three-dimensional arrow represents the magnetization in the CoFeB layer, while the green arrow denotes the magnetizations of Co in the GdCo layer.

S6. All-optical switching of $Gd_{25}Co_{75}$ (5 nm)/Cu (5 nm)/CoFeB (t nm) spin valves starting from AP^+ configuration

Fig. S6(a) demonstrates the MOKE images acquired from the Gd-rich $Gd_{25}Co_{75}$ (5 nm)/Cu (5 nm)/CoFeB (t nm) spin valves before and after irradiation with single laser pulses. Starting from the AP^+ configuration, three different Kerr contrast changes are observed, depending on t. The definition of Kerr configurations remains identical to that in the main text. Fig. S6(b) presents the corresponding Kerr contrast as a function of position along the radius of the circular irradiated region after the second pulse irradiation. In Fig. S6(c), the variation in magnetization of the CoFeB layer after the second single pulse, derived from the MOKE signal in the central region, is plotted against increasing t.

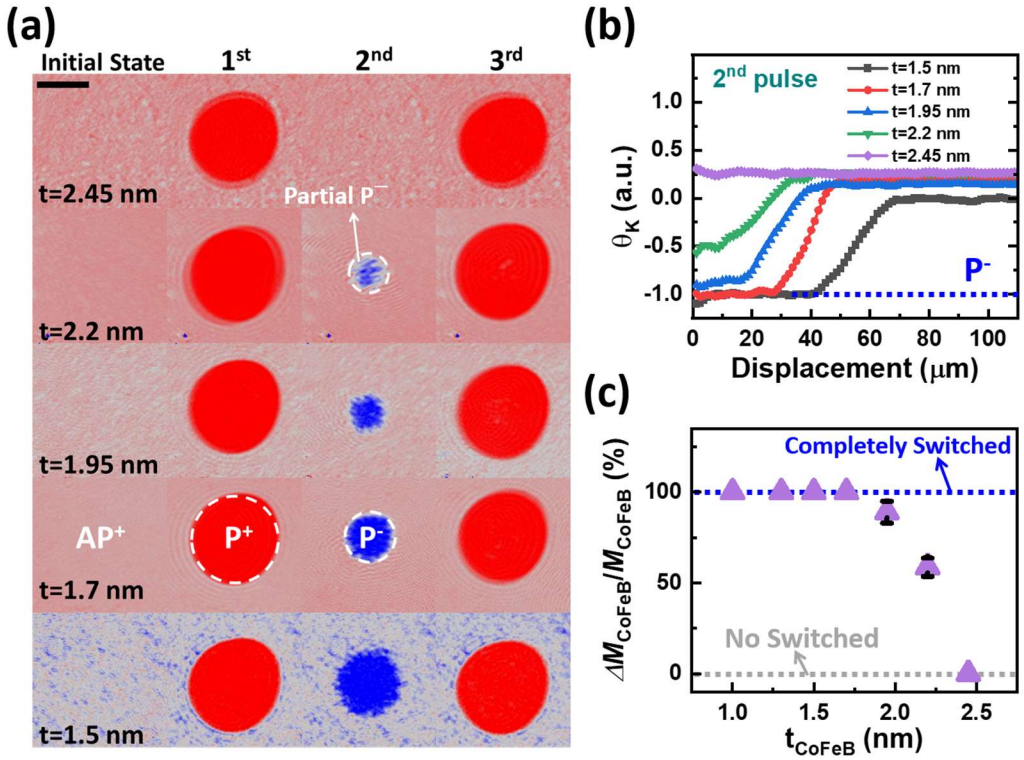

FIG. S6. All-optical switching for the Gd-rich $Gd_{25}Co_{75}$ (5 nm)/Cu (5 nm)/CoFeB (t nm) spin valves with various CoFeB layer thicknesses (t), starting from the initial state AP^+. (a) MOKE images acquired after irradiation with different numbers of laser pulses. The pulse fluences used in the measurements range between 8 to 11 $mJ \times cm^{-2}$. The scale bar is 100 μm long. (b) The Kerr contrast obtained following the second pulse excitation, is plotted as a function of the position from the center of the switching region. (c) The magnetization changes of CoFeB, estimated from the Kerr contrast changes after the second laser pulse excitation, are plotted as a function of t.

S7. Effect of insulator MgO insertion and laser pulse helicity on the single pulse reversal of CoFeB layer

To validate that our single pulse-induced full reversal of the in-plane magnetized CoFeB layer is attributed to the spin transport interpretation, we fabricated spin valves with and without MgO insertion in the Cu layer. The spin valve with the MgO layer is expected to block Gd spin currents. Our results demonstrate that the spin valve lacking the MgO layer displays both P^+ to P^- switching and P^+ to AP^+ switching induced by a single pulse. In contrast, the spin valve incorporating MgO insertion only presents switching in the GdCo layer after each pulse, while the CoFeB layer consistently shows a multidomain state (Multi) regardless of the pulse number applied. These findings indicate the necessity of Gd spin currents to achieve single pulse reversal of the CoFeB layer.

Moreover, we conducted AOS measurements with different polarizations of the pump pulse, including one linearly polarized and two helicities. The results show that the final state of the CoFeB magnetization is solely determined by the orientation between the magnetization of Gd and CoFeB, irrespective of the light polarization. Consequently, it can be concluded that the thermal origin of the Gd spin currents.

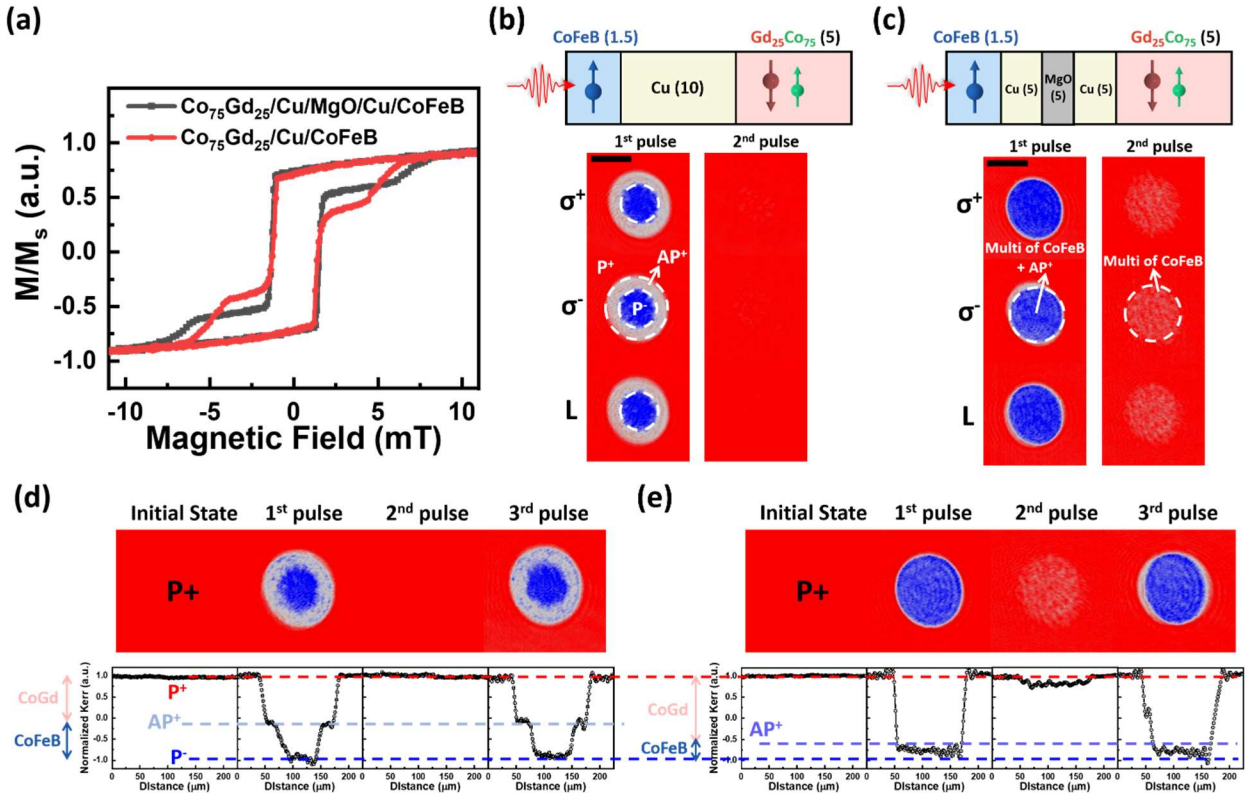

FIG. S7. (a) Comparison of magnetization curves for two samples with and without MgO insertion. AOS in Gd-rich $Gd_{25}Co_{75}$ (5 nm)/Cu (5 nm)/MgO (h nm)/Cu (5 nm)/CoFeB (1.5 nm) spin valves with (b) h=0 nm or (c) 5 nm. The simplified sample stacks are depicted above the Kerr images,

respectively. A laser pulse fluence of 11.26 mJ×cm^{-2} is utilized, with different pulse polarization: σ^+ (left circularly polarized light), σ^- (right circularly polarized light), and L (linearly polarized light). The experiments started from the P^+ configuration. The scale bar represents a length of 100 μm. MOKE images were taken after irradiation using L with varying pulse numbers for spin valves with (d) h=0 nm and (e) 5 nm. The corresponding Kerr contrast profiles are shown, and the dashed lines indicate different magnetic configurations.

S8. Absorption profile calculation with different CoFeB thickness

We conducted light absorption calculations using the Transfer Matrix Method to evaluate the variation in temperature rise with different CoFeB thicknesses (t) in the spin valves (Glass/Ta (3 nm)/GdCo (5 nm)/Cu (5 nm)/$Co_{40}Fe_{40}B_{20}$ (t nm)/Pt (3 nm)). Fig. S8(a) illustrates the calculated light absorption for the spin valve structure with various t values. Fig. S8(b) presents the total absorption in both the CoFeB layer and the GdCo alloy, respectively. The results indicate that absorption within the CoFeB layer increases with CoFeB thickness, while absorption within the GdCo layer slightly decreases with increasing CoFeB thickness.

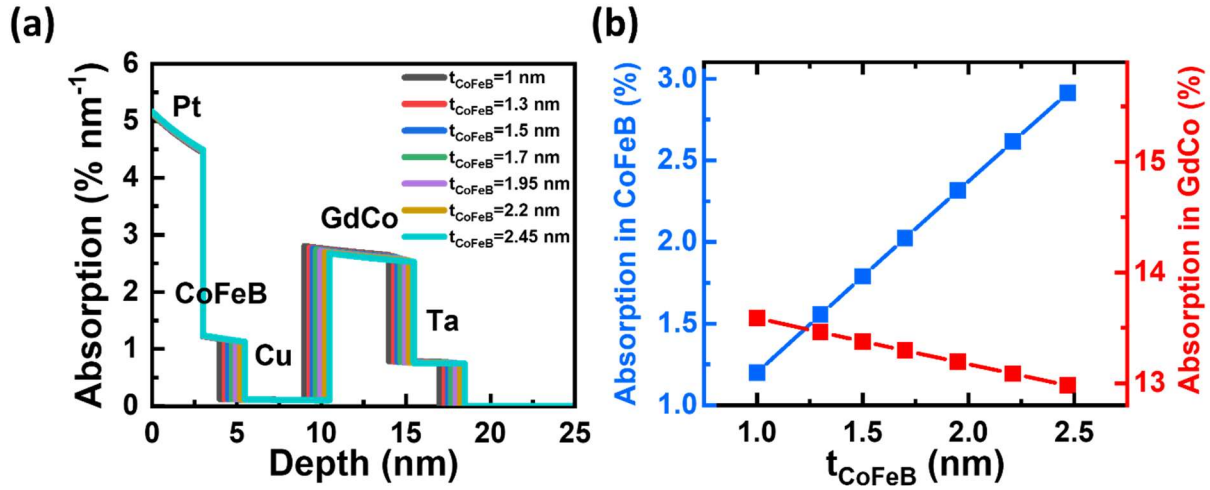

FIG. S8. (a) Optical absorption calculated as a function of depth for different CoFeB film thicknesses (t_{CoFeB}) in GdCo (5 nm)/Cu (5 nm)/CoFeB (t nm) spin valves. Total energy absorption in (b) the CoFeB layer and the GdCo layer, plotted as a function of t. The optical indices utilized in the calculations were obtained from a previous study [4,6].

Reference

1. S. Iihama, Y. Xu, M. Deb, G. Malinowski, M. Hehn, J. Gorchon, E. E. Fullerton, and S. Mangin, Single-shot multi-level all-optical magnetization switching mediated by spin transport, Adv. Mater. **30**, 1804004 (2018).
2. Q. Remy, J. Hohlfeld, M. Vergès, Y. Le Guen, J. Gorchon, G. Malinowski, S. Mangin, and M. Hehn, Accelerating ultrafast magnetization reversal by non-local spin transfer, Nat. Commun. **14**, 445 (2023).
3. Q. Remy, J. Igarashi, S. Iihama, G. Malinowski, M. Hehn, J. Gorchon, J. Hohlfeld, S. Fukami, H. Ohno, and S. Mangin, Energy efficient control of ultrafast spin current to induce single femtosecond pulse switching of a ferromagnet, Adv. Sci. **7**, 2001996 (2020).
4. J. Igarashi, Q. Remy, S. Iihama, G. Malinowski, M. Hehn, J. Gorchon, J. Hohlfeld, S. Fukami, H. Ohno, and S. Mangin, Engineering Single-Shot All-Optical Switching of Ferromagnetic Materials, Nano Lett. **20**, 8654 (2020).
5. E. Callen, and H. Callen, Ferromagnetic Transitions and the One-Third-Power Law, J. Appl. Phys. **36**, 1140 (1965).
6. X. Liang, X. Xu, R. Zheng, Z. A. Lum, and J. Qiu, Optical constant of CoFeB thin film measured with the interference enhancement method, Appl. Opt. **54**, 1557 (2015).